Bonding, Backbonding, and Spin-Polarized Molecular Orbitals:
Basis for Magnetism and Semiconducting Transport in V[TCNE]$_{x\sim2}$

J. B. Kortright,[1] D. M. Lincoln,[3] R. Shima Edelstein,[2] and A. J. Epstein[2,3]

[1]*Materials Sciences Division, Lawrence Berkeley National Laboratory,*
Berkeley, CA 94720-8099

[2]*Department of Physics, The Ohio State University, Columbus, OH 43210-1117*

[3]*Department of Chemistry, The Ohio State University, Columbus, OH 43210-1185*

Abstract

X-ray absorption spectroscopy (XAS) and magnetic circular dichroism (MCD) at the V $L_{2,3}$ and C and N K edges reveal bonding/backbonding interactions in films of the 400 K magnetic semiconductor V[TCNE]$_{x\sim2}$. In V spectra, d_{xy}-like orbitals are modeled assuming V^{2+} in an octahedral ligand field, while d_{z^2} and $d_{x^2-y^2}$ orbitals involved in strong covalent bonding cannot be modeled by atomic calculations. C and N MCD, and differences in XAS from neutral TCNE molecules, reveal spin-polarized molecular orbitals in V[TCNE]$_{x\sim2}$ associated with backbonding interactions that yield its novel properties.

Vanadium tetracyanoethylene (V[TCNE]$_{x\sim2}$) stands out in a broader class of condensed phase, molecule-based magnets [1, 2] by exhibiting magnetic ordering to 400 K [3], semiconducting magneto-resistive transport [4, 5], and photo-induced magnetism [6, 7]. These novel properties imply a distinct, spin-polarized electronic structure [4], but its details have remained elusive. While a nominal structural model for short-range order in V[TCNE]$_{x\sim2}$ has emerged [8], inherent structural disorder and metastability of both solution prepared powders [3] and solvent free chemical vapor deposition (CVD) films [9] have hindered thorough understanding of the electronic structure underlying its properties. The nominal structural model is based on a simple ionic picture with spin S = 3/2 V^{2+} coordinating octahedrally with 1 of the 4 N terminations of 6 different S = ½ TCNE$^{\bullet-}$ radical anion ligands. Long-range crystalline order is absent and the structure is network-like with TCNE$^{\bullet-}$ bridging V^{2+}, and *vice versa*. For x = 2 only ¾, on average, of the N of each TCNE$^{\bullet-}$ coordinate with V^{2+} to maintain charge neutrality. Recent V K edge EXAFS supports this model, yielding 6 N atoms at 2.08 Å from the central V^{2+} [8].

Several studies aim to elucidate this electronic structure. Photoemission spectroscopy of Rb intercalated TCNE [10] and V[TCNE]$_x$ [11, 12] shows metal-induced changes in TCNE valence states. X-ray absorption (XAS) and magnetic circular dichroism (MCD) spectroscopy at the V $L_{2,3}$ edges of V[TCNE]$_x$ [11, 12] were partially modeled by atomic multiplet calculations [12]. These studies were interpreted to imply strong but unspecified covalent bonding between V and TCNE with V in a mixed-valent, charge-transfer ground state consisting of $V^{2+} + V^{1+}L$ where L is a ligand hole on TCNE. While these studies advance knowledge of V[TCNE]$_{x\sim2}$, they leave important aspects of the V XAS spectra unexplained, do not provide a specific covalent bonding mechanism, and do not explore the role of TCNE in the spin-resolved electronic properties.

In this letter, we report XAS and MCD measurements at the V $L_{2,3}$ and C and N K edges in V[TCNE]$_{x\sim2}$ films and the C and N edges in isolated TCNE molecules. Our V results reveal

additional features compared to previous studies, leading to a very different interpretation. At the C

and N edges we observe changes in the molecular orbital (MO) structure of TCNE in V[TCNE]$_{x\sim2}$

films compared to gas-phase TCNE, including spin-polarized states near the Fermi level (E$_F$).

Combined results reveal interactions between V d states and TCNE MO states involving strong

covalent σ bonding and weaker, spin-polarized π backbonding.

V[TCNE]$_{x\sim2}$ films (100-200 nm thick) were deposited by CVD [9] onto SiN$_x$ membrane

substrates (100 nm thick), capped with Al (30 nm) to suppress oxidation, and sealed in evacuated

ampoules. At the Advanced Light Source samples were removed in N$_2$ and introduced into the

vacuum chamber with minimal air exposure. O K edge XAS revealed that some samples contained

observable O. Data reported here, however, are from samples showing no trace of O by XAS (Fig.

1a). XAS and MCD were measured in transmission at 298 K with circularly polarized x-rays

(degree of circular polarization ~ 0.85). An electromagnet applied an AC field (5 Hz, +/- 200 Oe

peak) to facilitate lock-in detection of weak MCD at the C and N edges. Fixed helicity MCD

features change sign on helicity reversal proving they are real. C and N XAS were also measured

from gas-phase, neutral TCNE (TCNE[0]) for comparison with films.

Vanadium XAS (Fig. 1b) resolves at least 4 L_3 multiplet peaks and 2 L_2 peaks, indicating

that a predominant V charge state and ligand field environment exist in V[TCNE]$_{x\sim2}$. This structure

is similar to, but more pronounced than, that in Ref. 12. Using atomic ligand field multiplet (LFM)

calculations (T = 0 K) we evaluated V^{n+} spectra for n = 1 - 3 in an octahedral ligand field (O_h) of

varying strength 10Dq [13]. The best result (Fig. 1b) is for V^{2+} ($d3$), consistent with expectations [9,

12], with 10Dq = 2.4 eV. Model spectra are broadened by a Gaussian of width 0.2 eV to simulate

experimental resolution, by Lorentzians of width 0.2(0.4) eV in the $L_3(L_2)$ regions to simulate

lifetime broadening, and a Fano line shape asymmetrically broadens the L_2 line to simulate

interference between 2$p_{1/2}$ and 2$p_{3/2}$ channels. While multiplets at the leading edge of both L_3 and

L_2 lines are reproduced, significant intensity not reproduced broadens measured lines to higher energy. This extra broadening was observed but not modeled in Ref. 12. We find that one broad Gaussian at each L_3 and L_2 line added to the LFM model accounts for all features and the entire width of the spectrum (Fig. 1d). These Gaussians account for 27% of the total XAS intensity of this new model.

The significance of these *ad hoc* Gaussians is of central importance, and not obvious *a priori*. Within LFM theory they could result as simple admixtures of different charge states or from charge transfer to or from ligands yielding different charge states that mix before evaluation of the dipole transition matrix element [13]. Indeed the Gaussians are located where V^{3+} multiplet structure would exist. We explored and do not adopt these models for several reasons. An added V^{3+} contribution would have its own multiplet structure that is not apparent in the data. Charge transfer models result in narrower multiplet lines compared to simple LFM models of comparable $10Dq$ [13] and cannot model the full spectral breadth. The sharp distribution of N about V^{2+} from V K EXAFS [8] is inconsistent with multiple valence states. The Gaussians are too large to be excited state satellites. We propose instead that they result from covalent bonding between V and TCNE that atomic multiplet theory cannot describe, and develop a covalent bonding model consistent with V, C and N XAS.

Covalent bonding is expected in organometallic molecules in which octahedrally coordinated transition metal ions interact with ligands through distinct σ bonding and π backbonding mechanisms. Aspects of this model have been considered for non-magnetic molecules containing V^{2+} [14] and for crystalline hexacyanometalate magnets [15, 16]. To investigate applicability of this general model to V[TCNE]$_{x\sim2}$, note that the V^{2+} LFM spectrum in Fig. 1b decomposes into 3 final state resolved symmetries [13]; 3-fold degenerate T_1 states describe transitions into the d_{xy}, d_{xz}, and d_{yz} orbitals while 1-fold A_1 and A_2 states describe transitions into the

d_{z^2} and $d_{x^2-y^2}$ orbitals and account for 33% of the XAS intensity. Hybridization associated with strong covalent σ bonding would redistribute d_{z^2} and $d_{x^2-y^2}$ states into bonding/antibonding states not describable by atomic theory. Weaker π interactions, however, might yield T_1 contributions approximated by LFM models. Indeed the T_1 spectrum itself approximates that measured with $10Dq = 2.25$ eV (Fig. 1e). Gaussians added to this T_1 spectrum yield a good approximation of the V XAS, where now they are identified with transitions into empty A_1 and A_2 states hybridized into σ^* states ~5 eV above E_F. This is consistent with covalent σ bonding between d_{z^2} and $d_{x^2-y^2}$ states and the lone pair electrons localized in TCNE$^{\bullet-}$ σ MOs, and much weaker interaction between the T_1 states and the TCNE$^{\bullet-}$ π MO system.

V MCD data are modeled equally well by the full V^{2+} LFM model (Fig. 1c) and the T_1-only LFM model (Fig. 1f). Calculations reveal that transitions into T_1 states account for all MCD at T = 0 K and most MCD at 300 K. Even without sum rule analysis to separate spin (m_s) from orbital (m_l) moments [17, 18], the comparable size of measured and model MCD confirms that V^{2+} is essentially fully spin polarized in a high-spin configuration ($m_s = 3$, S = 3/2) key to the high T_C of V[TCNE]$_{x\sim2}$. The ratio $m_l/m_s \cong -0.01$, with m_l opposing m_s as expected by Hund's rules.

XAS at the C and N K edges of TCNE^0 reveals a well-defined MO structure with 3 π^* peaks in each spectrum (Fig. 2) representing transitions from localized $1s$ atomic levels into the 3 lowest unoccupied MO (LUMO) states having characteristic empty density of states (DOS) distributions extending across the molecule [19, 20, 21]. C and N spectra probe the 3 LUMOs from different sites within the molecule. The 1st peak results from transitions to the lowest π^* MO with DOS antinodes out of the molecular plane and lobes localized near the central C_1 and the N sites (Fig. 2 inset). The 2nd and 3rd peaks result from transitions to 2 π^* MO states associated more with the $C_2\equiv N$ triple bonds. The splitting between the 1st and 2nd peaks differs at the C and N edges, while

that between the 2nd and 3rd peaks is identical; this results from different screening of C_1 and C_2 sites contributing to the 1st and to the 2nd and 3rd peaks, respectively.

C and N XAS spectra of V[TCNE]$_{x\sim2}$ show significant similarities and differences compared to those of TCNE^0 (Fig. 3a & 3b). The TCNE^0 2nd and 3rd LUMO peaks remain intact, albeit significantly broadened, in V[TCNE]$_{x\sim2}$. The 1st LUMO in the C spectra splits into 2 peaks, while 3 peaks can be resolved in the low energy region of the N spectra (below). We measure 16 and 48% reduction, respectively, in C and N empty π^* state density in V[TCNE]$_{x\sim2}$ compared to TCNE^0 [22], consistent with charge transfer from V to TCNE such that more added charge resides near the more electronegative N sites. These results reveal interaction-induced changes in the LUMO of TCNE^0 and also imply that its planar geometry and general structure of TCNE^0 remain intact in V[TCNE]$_{x\sim2}$.

MCD is observed at the C and N edges (Figs. 3c & 3d) providing the first evidence of spin polarization of the TCNE$^{\bullet-}$ π system in V[TCNE]$_{x\sim2}$. Its small size results from weak 2p spin-orbit coupling and no spin-orbit splitting in the 1s levels, implying that K edge MCD senses only m_l and not m_s [23]. Even with low S/N, distinct MCD is apparent in the lower part of the π^* region where XAS splitting exists. C MCD shows positive and negative peaks at 284 and 285 eV, respectively. N MCD shows positive and negative peaks at 397 and 398 eV, respectively.

Further insight into the V[TCNE]$_{x\sim2}$ electronic structure comes from collecting C, N, and V spectra as in Fig. 4, where each is plotted over a 10 eV range to roughly align E_F for each element. Such alignment is approximate ($\pm$ 0.5 eV) because of general uncertainty in E_F and different chemical shifts of distinct C and N sites. Even so, clear correlations further support the bonding/backbonding model. The Gaussians in the V XAS spectrum fall just above the former 3rd LUMO in the C and N spectra in the TCNE σ^* region, consistent V σ^* states and explaining their

width. Photoemission reveals an enhancement of filled DOS roughly 6 eV below E_F [12] that would

correspond to the bonding counterpart of this interaction. The coincidence of specific features in

the TCNE$^{\bullet-}$ π^* and the V T_1 spectra is consistent with backbonding interactions.

In the former 1st LUMO region in V[TCNE]$_{x\sim2}$, 2 and 3 peaks can be resolved at the C and

N edges, respectively (Figs. 4b, 4c insets). 0.7 eV separates these peaks at both edges. For C this

region is dominated by transitions from the central C_1 sites, while for N 2 distinct sites contribute,

only ¾ of which coordinate with V. This multiplicity of N sites explains why 3 peaks are resolved

for N while only 2 are resolved for C. In Fig. 4 the 2 split peaks in the C spectrum are aligned to

the 2nd and 3rd split peaks in the N spectrum.

The opposite MCD of the 2 peaks in the C spectrum leads us to consider whether magnetic

exchange between V and TCNE accounts for the 0.7 eV splitting. Charge transfer from V to TCNE

yields a singly-occupied former LUMO that splits into spin-polarized sub-bands in a magnetic

sample. The magnetic exchange energy in V[TCNE]$_{x\sim2}$ [24, 25] is more than 10 times smaller than

the observed splitting. Rather than exchange splitting, we note the observed value is of the same

order as the V T_1 multiplet splitting. Thus backbonding interactions between relatively unperturbed,

spin-polarized V d_{xy}-like states and more strongly perturbed TCNE π^* MO states can account for

the former LUMO splitting.

Magnetism and activated transport in V[TCNE]$_{x\sim2}$ are explained by a large imbalance in

occupation of spin-split sub-bands of the TCNE$^{\bullet-}$ former LUMO. TCNE$^{\bullet-}$ spins in the occupied,

lower sub-band align antiparallel to V^{2+} spins in weakly hybridized backbonding levels, yielding

ferrimagnetic alignment of TCNE$^{\bullet-}$ and V^{2+} spins. The empty, upper sub-band is then spin-aligned

with filled V^{2+} d states at E_F, yielding semiconducting transport with activation energy close to the

measured value of 0.5 eV [4, 5]. Coulomb repulsion within the π^* levels [4] may contribute to the energy splitting along with hybridization.

While disorder precludes the use of polarized XAS to measure relative orientation of V^{2+} and TCNE$^{\bullet-}$ backbonding orbitals, they are largely predicted by this model. In a reference frame with V^{2+} centered in a cube and the d_{z^2} and $d_{x^2-y^2}$ orbitals pointing to face centers, σ bonding orients 1 of the 4 arms of each of the 6 ligands along 3 orthogonal V-N-C$_2$ axes. V d_{xy}-like orbitals point toward cube edge centers, and backbonding interactions with π MOs of a given TCNE$^{\bullet-}$ depend on its azimuthal orientation about its σ bond axis. When its π lobes point toward the cube edge centers they have maximum overlap with d_{xy}-like orbitals, and a given d_{xy}-like lobe overlaps with so-oriented π lobes from 1 or 2 different TCNE$^{\bullet-}$ ligands. Alternatively, π orbitals that align toward the cube corners overlap with 2 different d_{xy}-like orbitals from the same V^{2+} center. Disorder in this azimuthal degree of freedom yields a range of backbonding interactions broadening the C and N π^* peaks, as observed, and coupled with steric hindrance of planar TCNE$^{\bullet-}$ ligands explains the lack of crystallinity.

In summary, combined C, N and V XAS and MCD reveal bonding/backbonding interactions in V[TCNE]$_{x\sim2}$ that explain its novel electronic properties with a detailed and predictive electronic structure. Strong covalent σ bonding holds V^{2+} and TCNE$^{\bullet-}$ constituents together while weaker π backbonding interactions mediate combined magnetic and semiconducting transport properties. This model can be tested with further x-ray and other experimental studies in this and related systems, and provides a clear starting point for density functional theory studies of material properties and to yield more realistic models of measured x-ray spectra in mixed metal/organic systems in which mixed ionic and covalent bonding limits applicability of atomic models.

Acknowledgements

References

1 J. S. Miller, and A. J. Epstein, Chem. Comm. 1319 (1998).

2 A. J. Epstein, MRS Bull. **28**, 492 (2003).

3 J. M. Manriquez, *et al.*, Science **252**, 1415 (1991).

4 V. N. Prigodin, *et al.*, Adv. Mater. **14**, 1230 (2002).

5 N. P. Raju, *et al.*, J. Appl. Phys. **93**, 6799 (2003).

6 J. W. Yoo, *et al.*, Phys. Rev. Lett. **97**, 247205 (2006).

7 J. W. Yoo, *et al*., Phys. Rev. Lett. **99**, 157205 (2007).

8 D. Haskel, *et al*., Phys. Rev. B **70**, 054422 (2004).

9 K. I. Pokhodnya, A.J. Epstein, and J. S. Miller, Adv. Mat. **12**, 410 (2000).

10 C. Tengstedt, *et al.*, Phys. Rev. B **69,** 165208 (2004).

11 C. Tengstedt, *et al*., Phys. Rev. Lett. **96**, 057209 (2006).

12 M. P. de Jong, *et al.*, Phys. Rev. B **75,** 064407 (2007).

13 F. de Groot and A. Kotani, *Core Level Spectroscopy of Solids* (CRC Press, Boca Raton, 2008).

14 P. Frank, *et al.*, Inorg. Chem. **41**, 3269 (2002).

15 T. Mallah, *et al*., Science **262**, 1554 (1993).

16 W. R. Entley and G. S. Girolami, Science **268**, 397 (1995).

17 P. Carra, *et al*., Phys. Rev. Lett. **70**, 694 (1993).

18 Close spacing of V L_3 and L_2 lines hinders separation of their MCD components in sum rule analysis to separate m_s and m_l. m_l/m_s can be determined.

19 A. Zheludev *et al.*, J. Am. Chem. Soc. **116**, 7243 (1994).

20 M.-J. Hubin-Franskin, *et al.*, J. Chem. Phys. **106**, 35 (1997).

21 C. I. Oprea, A. Damian, and M. A. Girtu, J. Optoelectronics & Adv. Mat. **8**, 191 (2006).

22 After renormalizing C(N) spectra to have the same edge jump, areas of π^* peaks are proportional to empty π state density.

23 G. Y. Guo, J. Phys. Cond. Matt. **8**, L747 (1996).

24 A. J. Epstein and J. S. Miller, Mol. Cryst. Liq. Cryst. **233**, 171 (1993).
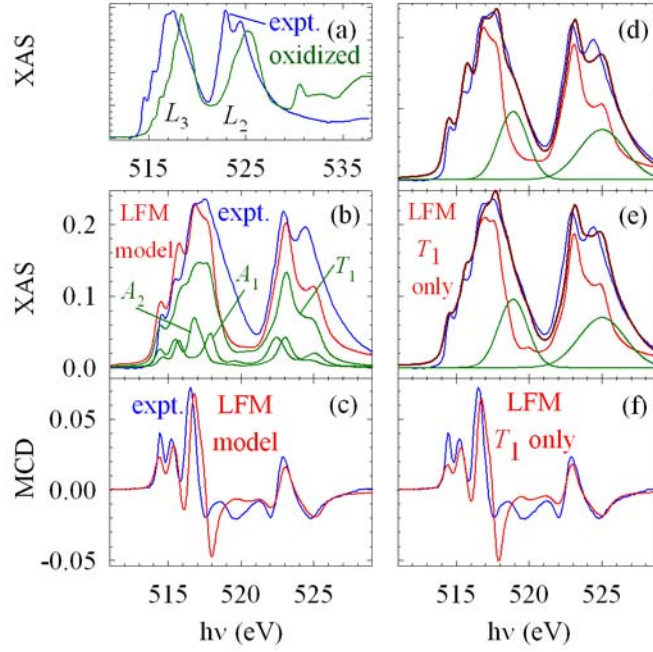
25 K. Koizumi, *et al.*, Polyhedron **24**, 2720 (2005).

Figure 1. (Color online) Measured V $L_{2,3}$ edge XAS and MCD (blue). (a) compares XAS from an intentionally oxidized sample (green) with a fresh sample. (b) and (c) show calculated XAS and MCD for a full LFM model assuming V^{2+} in O_h with $10Dq = 2.4$ eV. The same vertical scaling factor has been applied to both XAS and MCD spectra. In (d) the model (dark red) is the sum of the same LFM spectrum and 2 Gaussians shown (green). (e) and (f) include just the T_1 component of an LFM model with $10Dq = 2.25$ eV.
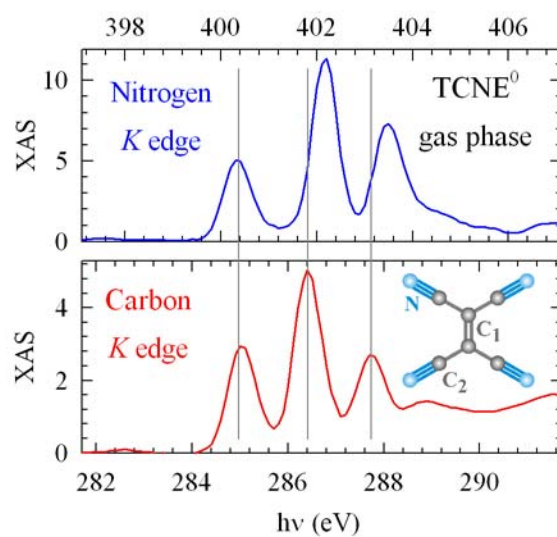
Figure 2. (Color online) C and N XAS of $TCNE^0$. Energy scales align the 1st peaks and each spectrum spans 10 eV. Vertical lines are visual guides. Ball and stick model of $TCNE^0$ (insert).
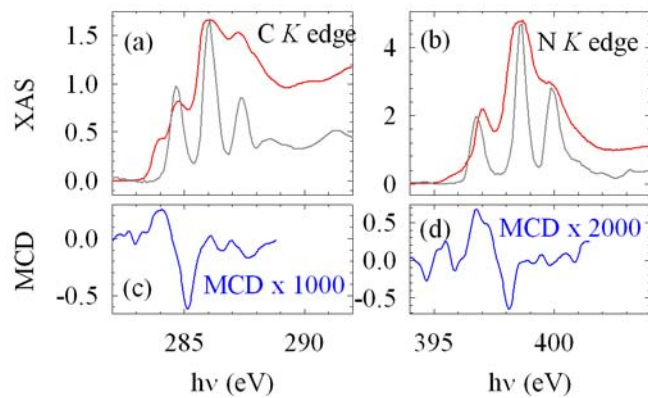
Figure 3. (Color online) C (left) and N (right) XAS and MCD spectra for V[TCNE]$_{x\sim 2}$ are in the top and bottom panels, respectively. Scaled XAS spectra from TCNE^0 (grey) are included.
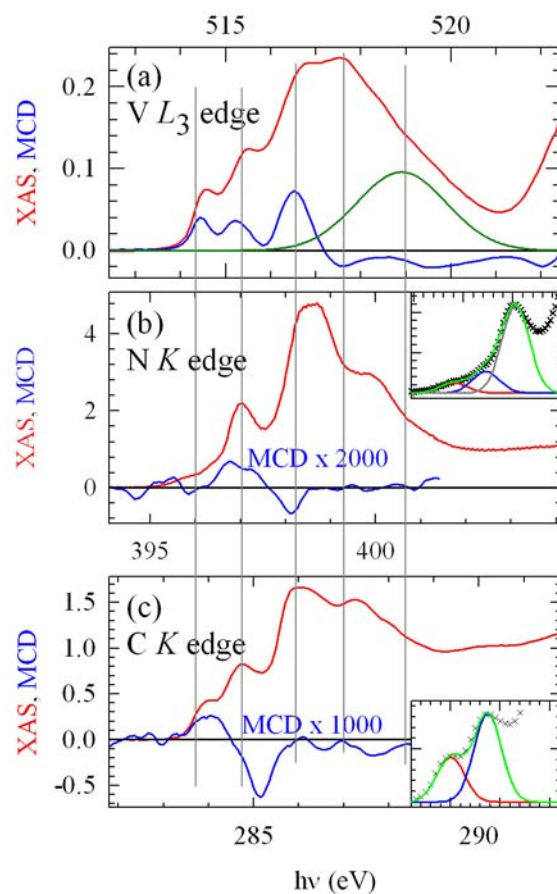
Figure 4. (Color online) XAS (red) and MCD (blue) at all 3 edges in V[TCNE]$_{x\sim2}$, (see text for vertical alignment). Insets in (b) and (c) show Gaussian fits to the low energy XAS regions. (a) includes the Gaussian representing transitions into σ^* states in the bonding/backbonding model. Vertical lines are visual guides.